*Proc. Natl. Acad. Sci. USA*
Vol. 89, pp. 8552–8556, September 1992
Neurobiology

# Alternative splicing generates functionally distinct *N*-methyl-D-aspartate receptors

(glutamate receptor/alternative RNA splicing/cerebellum/molecular cloning)

NOBUKI NAKANISHI, RICHARD AXEL, AND NEIL A. SHNEIDER

Department of Biochemistry and Molecular Biophysics, and the Howard Hughes Medical Institute, College of Physicians and Surgeons, Columbia University, New York, NY 10032

*Contributed by Richard Axel, June 15, 1992*

**ABSTRACT** **We have used expression cloning in *Xenopus* oocytes to isolate two different cDNAs encoding functional *N*-methyl-D-aspartate (NMDA) receptor subunits. The two receptors (NMDA-R1A and -R1B) display different pharmacologic properties as a consequence of alternative exon addition within the putative ligand-binding domain. The splicing choice is regulated such that R1B is the predominant form of receptor in the cerebellum, whereas R1A predominates in other brain regions. Expression of either of the subunits alone in oocytes results in an NMDA-evoked inward current with electrophysiologic properties closely resembling those of the NMDA receptors observed in neurons. Thus, the complex properties exhibited by the NMDA receptor in neurons can be generated by the expression of a single receptor subunit.**

The amino acid glutamate is the major excitatory neurotransmitter in the vertebrate central nervous system. The subclass of glutamate receptors responsive to *N*-methyl-D-aspartate (NMDA) exhibits several interesting properties (1–3). (*i*) The NMDA receptor has an obligate requirement for glycine and glutamate for channel activation (4, 5). (*ii*) NMDA activates a large conductance cation channel that is permeable to $Ca^{2+}$ as well as to monovalent ions (6–9). (*iii*) The channel is blocked by extracellular $Mg^{2+}$ ions at resting potentials (6, 10). When the membrane is depolarized, the $Mg^{2+}$ block is relieved and the receptor can be activated by glutamate. Activation of the NMDA receptor therefore requires the association of two synaptic events, membrane depolarization and glutamate release. This associative property may provide the logic for the role of the receptor in synaptic plasticity during development and learning (11, 12). In addition, the $Ca^{2+}$ influx through the NMDA receptor may, in part, be responsible for the neurotoxic actions of glutamate (13).

One approach to understanding the complex properties of the NMDA receptor involves the cloning and characterization of the genes encoding this receptor. Recently, Moriyoshi *et al.* (14) used expression cloning to isolate a cDNA clone encoding an NMDA-responsive glutamate receptor subunit. In a separate study, the mouse homologue of this subunit was isolated by low stringency hybridization (15). In this study, we have independently used expression cloning in *Xenopus* oocytes to isolate two distinct functional cDNAs encoding NMDA receptor subunits. One clone (NMDA-R1A) is identical to that reported recently (14, 15), whereas the second clone (NMDA-R1B) contains an additional 21-amino acid exon within the N-terminal extracellular domain. Thus, alternative splicing contributes to NMDA receptor diversity.

## METHODS

**PCR Amplification of the Glutamate Receptor Homologues and Hybrid Depletion.** Single-stranded cDNA synthesized from rat forebrain poly(A)$^+$ RNA was used in a standard PCR reaction (Perkin–Elmer) with the two degenerate primers CGGAATTCGGIGGI(A/G)TITGGTGGTT(C/T)TT(C/T)AC (upstream) and GCCTCGAGTCITCIGCI(C/G)(A/T)ITCIATIGG (downstream, I = inosine). These primers amplify the region between residues 598 and 634 of glutamate receptor 1 subunit (GluR1; indicated by arrows in Fig. 1*A*). Plasmids containing these PCR products described above were first linearized by *Bam*HI restriction digestion. Antisense RNA was transcribed from the linearized plasmids in standard reactions (16) containing 1 mM bio-11-UTP (ENZO). Fifty nanograms of biotinylated antisense RNA was then hybridized to 3 μg of rat forebrain poly(A)$^+$ RNA in 10 μl of RNA hybridization buffer (40 mM Hepes, pH 6.4/400 mM NaCl/1 mM EDTA/80% formamide) at 45°C for 4 hr. As an internal control, 30 ng of capped sense RNA from each of the α, β, γ, and δ subunits of the mouse nicotinic acetylcholine receptor was added in the hybridization mixture. After hybridization, the mixture was diluted with 190 μl of 10 mM Tris·HCl, pH 7.5/5 mM EDTA/300 mM NaCl and then extracted twice with phenol/chloroform/isoamyl alcohol (24:24:1). mRNA that did not hybridize to the antisense RNA was recovered from the aqueous phase by ethanol precipitation and injected into *Xenopus* oocytes. After 4–6 days of incubation, the ratio of the amplitude of the NMDA-evoked response to that of the acetylcholine-evoked current was measured by voltage clamp recording for each oocyte as described (16).

**Hybrid Selection.** To select for mRNA species that hybridize to GluR7PCR (see *Results*), hybridization and phenol extraction were performed as described above. Duplex RNA was recovered from the organic phase by back extraction with an equal volume of salt-free buffer (10 mM Tris·HCl, pH 7.5/5 mM EDTA). After three rounds of extraction, the recovered aqueous phase was heated at 98°C for 10 min to denature the RNA duplexes. Immediately after heat treatment, the salt concentration of the solution was increased to 300 mM NaCl and the solution was extracted with phenol/chloroform/isoamyl alcohol to remove denatured antisense RNA.

**Construction and Screening of cDNA Libraries.** Directional cDNA libraries were constructed from size-selected rat brain poly(A)$^+$ RNA or hybrid-selected RNA in the vector λ Shlox. Low stringency hybridization using the radiolabeled GluR7PCR probe was performed at 42°C in 10% formamide/1% SDS/1 M NaCl/10% dextran sulfate/100 mg of salmon sperm DNA per ml. Filters were washed at 42°C in 10% formamide/1% SDS/1 M NaCl. Positive phage clones were converted to plasmids by an *in vivo* excision protocol (Novagen).

The publication costs of this article were defrayed in part by page charge payment. This article must therefore be hereby marked "*advertisement*" in accordance with 18 U.S.C. §1734 solely to indicate this fact.

Abbreviations: NMDA, *N*-methyl-D-aspartate; GluR1, glutamate receptor 1 subunit; APV, 2-amino-5-phosphonovaleric acid; *I–V*, current–voltage.

**Solutions.** Barium Ringer's solution is 20 mM $BaCl_2$/65 mM NaCl/2 mM KCl/5 mM Hepes, pH 7.4. When barium was replaced with 2 mM $CaCl_2$, NaCl concentration was increased to 95 mM.

## RESULTS

**Isolation and Structure of NMDA-R1 cDNAs.** Our initial experiments were based upon the assumption that significant homology might exist between the family of non-NMDA (16–25) and NMDA-responsive glutamate receptors. Degenerate primers within the most highly conserved region of the non-NMDA receptors were used in PCRs with rat forebrain poly(A)$^+$ RNA to generate eight different PCR products representing eight different non-NMDA receptor cDNAs. Each of the cloned PCR products was used in a hybrid depletion assay with forebrain poly(A)$^+$ RNA to determine whether any of these clones could anneal with RNA encoding the NMDA receptor. When the PCR product, GluR7PCR, was annealed with forebrain poly(A)$^+$ RNA, the NMDA-evoked current was diminished 50–60% in *Xenopus* oocytes. Subsequent experiments demonstrated that GluR7 does not encode an NMDA receptor but rather a non-NMDA receptor subunit (24). Forebrain RNA that hybridized with the GluR7PCR product was recovered and used to generate an enriched cDNA expression library comprised of $1.4 \times 10^5$ independent clones. RNA synthesized *in vitro* from this expression library generated an NMDA-evoked current when injected into *Xenopus* oocytes.

A second cDNA expression library was constructed from size-selected 4- to 5-kilobase (kb) forebrain poly(A)$^+$ RNA. RNA transcribed *in vitro* from this library also elicited an NMDA-evoked current when injected into oocytes. Interestingly, however, the pharmacological properties of the two NMDA-responsive channels from each of the two libraries were distinct. Although the response observed with RNA from both libraries required NMDA and glycine, the sensitivity to the competitive NMDA antagonist, DL-2-amino-5-phosphonovaleric acid (DL-APV) was different. The receptor subunit encoded in the library from hybrid-selected RNA was more sensitive to APV than the subunit present in the size-selected library. We therefore pursued the isolation of the NMDA receptor cDNAs from both expression libraries.

The size-selected library was serially diluted by sib selection (26) to obtain a pool of 200 independent clones containing a functional NMDA receptor cDNA, as determined by expression in *Xenopus* oocytes. This pool was screened by hybridization with the GluR7PCR probe at low stringency, and a positive clone was isolated. RNA transcribed from this clone expressed a functional NMDA receptor in oocytes. This clone (NMDA-R1A) was used to screen a pool of 1400 clones from the library constructed from hybrid-selected RNA. A second clone, NMDA-R1B, encoding functional NMDA receptor with distinct pharmacologic properties, was isolated. The DNA sequence of NMDA-R1A was identical to the sequence of NMDA-R1 described by Moriyoshi *et al.* (14). The deduced amino acid sequence reveals an open reading frame of 938 residues that shares 26.4% identity with the non-NMDA glutamate receptor subunit, GluR1 (Fig. 1*A*).

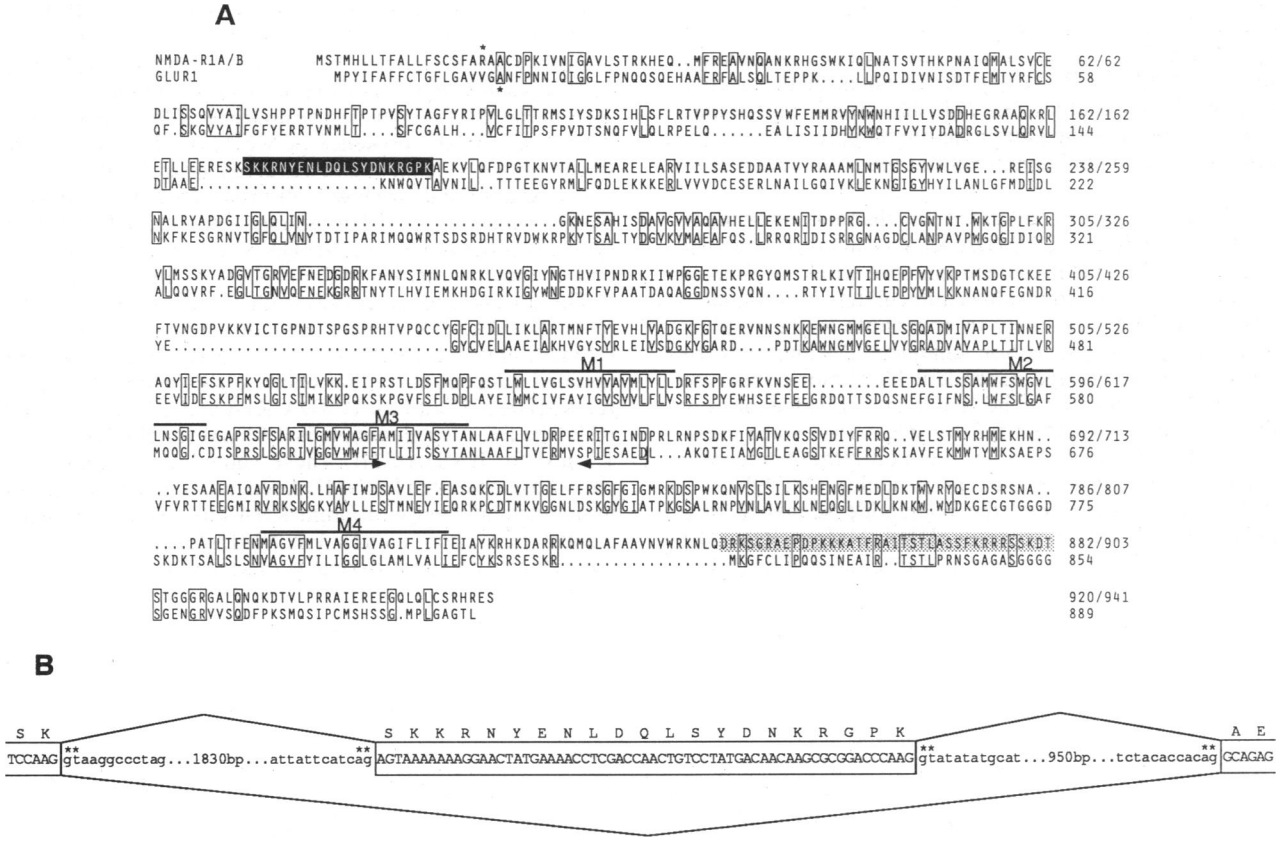


FIG. 1. Sequence of two functionally distinct NMDA receptor cDNA clones. (*A*) Alignment of the deduced amino acid sequences of rat NMDA-R1 and the non-NMDA glutamate receptor GluR1 (17). Numbers to the right of the NMDA-R1 sequence refer to the NMDA-R1A and -R1B residues, respectively. The NMDA-R1B-specific residues (amino acids 173–193) are in black. Boxed amino acid residues indicate identity between NMDA-R1 and GluR1. The 37-amino acid stretch shaded lightly near the C terminus of NMDA-R1 is deleted in the NMDA-R1C cDNA. (*B*) Organization of introns and exons surrounding the 63-base-pair (bp) exon specific to NMDA-R1B. Exon sequences are boxed and are shown in uppercase letters; intron sequences are represented in lowercase letters. The upper portion depicts the splicing pattern identified in NMDA-R1B cDNA, whereas the lower portion depicts the splicing pattern observed for NMDA-R1A cDNA.

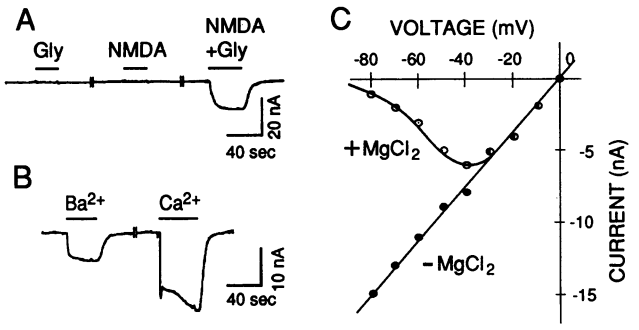


FIG. 2. Electrophysiological characterization of the NMDA-R1B receptor. (*A*) Voltage-clamp recording from a single *Xenopus* oocyte injected 4 days earlier with 10 ng of synthetic NMDA-R1B RNA. The oocyte membrane potential was maintained at −80 mV, and the oocyte was perfused with $Ba^{2+}$-Ringer's solution. Ten micromolar glycine alone (left), 100 μM NMDA alone (middle), or 100 μM NMDA and 10 μM glycine (right) was applied to the oocyte by superfusion for the duration indicated by the bars. (*B*) The oocyte was exposed to 100 μM NMDA and 10 μM glycine in either $Ba^{2+}$-Ringer's solution (left) or $Ca^{2+}$-Ringer's solution (right). (*C*) The current evoked by 100 μM NMDA and 10 μM glycine was plotted as a function of membrane potential in the absence (●) and presence (○) of 100 μM $Mg^{2+}$.

Assuming that NMDA-R1A conforms to the proposed structure of other ligand-gated ion channels, we predict that this receptor consists of a 540-residue N-terminal extracellular domain. This putative extracellular ligand-binding domain is followed by four transmembrane domains and a C-terminal 105-amino acid extracellular domain. As we previously observed for the non-NMDA receptor subunits (16), a block of about 140 residues in the N-terminal extracellular domain (residues 389–525 in R1A) and 40 residues in the second cytoplasmic loop (residues 732–774) share significant homology with the periplasmic glutamine-binding protein of *Escherichia coli*, an essential component of the glutamine permease.

By analogy to other ligand-gated ion channels, transmembrane domain 2 (M2) of NMDA-R1A is likely to line the channel pore (27). This presumed ion pore would be flanked by six negatively charged residues immediately N-terminal to M2. These residues are likely to contribute to the conductance properties of the cation channel (27) and may be responsible for the voltage-dependent $Mg^{2+}$ block observed for the NMDA receptor. The asparagine residue present within M2 may be important for ion selectivity, since mutations at the equivalent site in the non-NMDA receptor subunits dramatically alter $Ca^{2+}$ permeability (28, 29).

We have also determined the nucleotide sequence of a second functional NMDA receptor cDNA, NMDA-R1B. The sequence of NMDA-R1B is identical to that of NMDA-R1, except for a 63-bp insertion that introduces 21 additional amino acid residues at position 173 within the N-terminal extracellular domain (Fig. 1*A*). We have used PCR and sequence analysis of genomic DNA to determine the intron–exon structure in this region of the NMDA-R1 gene. This analysis demonstrates that the 63-bp insert is encoded by a distinct exon that is included in NMDA-R1B but remains part of an intron that is spliced out to generate NMDA-R1A (Fig. 1*B*).

**Electrophysiologic Properties of NMDA-R1A and -R1B in *Xenopus* Oocytes.** The function of the two NMDA receptor subunits was examined by voltage-clamp analysis in *Xenopus* oocytes. The electrophysiological properties of NMDA-R1A and -R1B were indistinguishable in our analyses. When oocytes injected with either NMDA-R1A or NMDA-R1B RNA were exposed to NMDA (100 μM) and glycine (10 μM), an inward current was evoked (Fig. 2*A*) similar in form to that observed in oocytes injected with unfractionated brain mRNA (30, 31). No current was observed when either of the two ligands was applied alone (Fig. 2*A*), demonstrating an obligate requirement for NMDA and glycine. Exposure of injected oocytes to NMDA and glycine in the absence of $Ca^{2+}$ generates a nondesensitizing inward current (Fig. 2*B*, left). In the presence of $Ca^{2+}$, however, a transient current peak followed by a slowly increasing inward current is also observed (Fig. 2*B*, right). These components of the NMDA-evoked current are likely to result from $Ca^{2+}$ flux through the NMDA receptor and the activation of $Ca^{2+}$-dependent $Cl^-$ channels present within oocyte membranes (32). We therefore carried out all subsequent pharmacologic analyses with Ringer's solution in which $Ca^{2+}$ was replaced by $Ba^{2+}$, permitting more quantitative measurements of NMDA receptor activation.

Both channels display a voltage-dependent $Mg^{2+}$ block. The current–voltage (*I–V*) relationship (shown for NMDA-R1B in Fig. 2*C*) is linear in the absence of $Mg^{2+}$ and reverses near 0 mV. In the presence of $Mg^{2+}$, the *I–V* curve is near linear above −30 mV and reverses near 0 mV. At more negative potentials (below −30 mV), the *I–V* response displays a negative slope. This voltage-dependent $Mg^{2+}$ block is typically observed for the NMDA receptors in neurons (6, 10) and in oocytes injected with poly(A)$^+$ brain mRNA (30, 31).

The dose–response curves with the agonists and antagonists, NMDA, L-glutamate, glycine, and D-APV reveal differences between NMDA-R1A and -R1B (Fig. 3). The $EC_{50}$ (agonist concentration that elicits a half-maximal response) for NMDA is 12 μM for NMDA-R1A and 26 μM for NMDA-R1B; the $EC_{50}$ for glutamate is 0.64 μM for NMDA-R1A and 1.1 μM for NMDA-R1B. These values are in good accord with those observed for NMDA receptors in neurons (33) and in oocytes injected with brain RNA (30). The differences in agonist activation curves for NMDA-R1A and -R1B are consistent with the differences observed in response to the

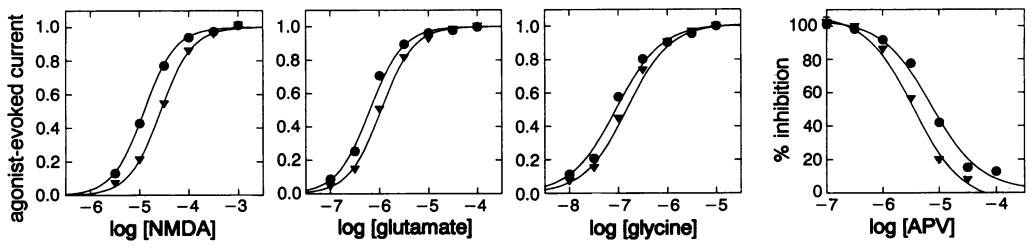


FIG. 3. Pharmacological characterization of the NMDA-R1A and NMDA-R1B receptors. Dose–response curves for NMDA, L-glutamate, glycine, and the NMDA antagonist D-APV were obtained from oocytes injected with 10 ng of synthetic NMDA-R1A (●) or -R1B (▼) RNA. NMDA and L-glutamate dose–responses were measured in the presence of 10 μM glycine. Glycine responses were recorded with 100 μM NMDA. Each point represents the mean current measured from five oocytes. The standard error of mean (SEM) is smaller than the symbol size for all data points. The curves are the least square fit of the data to the logistic equation (16). Responses were normalized to the maximum current values ($I_{max}$) derived from this analysis. D-APV was applied together with 100 μM NMDA and 10 μM glycine. Each point represents the mean current ($n$ = 5) as a percentage of the control current elicited by 100 μM NMDA and 10 μM glycine in the absence of D-APV.

competitive antagonist D-APV. At a fixed concentration of NMDA (100 $\mu$M) and glycine (10 $\mu$M), the $IC_{50}$ (antagonist concentration that produces 50% inhibition) of D-APV is 3.6 $\mu$M for NMDA-R1B and 7.2 $\mu$M for NMDA-R1A. Thus the R1A channel is more sensitive to the agonist NMDA than R1B. More subtle differences are observed in the glycine activation curves; the $EC_{50}$ is 77 nM for NMDA-R1A and 120 nM for NMDA-R1B. The Hill coefficients derived from each of the dose–response curves for NMDA, glutamate, and glycine were 1.3 for NMDA-R1A and NMDA-R1B. Taken together, these data demonstrate that the two forms of NMDA receptor subunits we have isolated exhibit significant differences in the response to agonists. The addition of a 21-amino acid exon in the presumed ligand-binding domain of NMDA-R1B may alter the affinity for glutamate and glycine. Although the results are consistent with conformational differences that alter the affinity for neurotransmitter, we cannot exclude the possibility that binding affinities are unaltered and the different dose–response curves result from differences in the gating properties of the two NMDA receptors.

**Expression of NMDA-R1A and -R1B.** We have used an RNase protection assay and *in situ* hybridization to determine the sites of expression of the two NMDA receptors we have cloned. RNase protection experiments permit a quantitative determination of the relative levels of expression of the NMDA-R1A and -R1B in various brain regions. A 266-nucleotide radiolabeled RNA probe, spanning the 63-nucleotide exon unique to NMDA-R1B (Fig. 4), was annealed with RNA from cerebral cortex, hippocampus, cerebellum, and olfactory bulb. When this RNA probe is annealed with synthetic R1B RNA, an intact 266-nucleotide fragment is protected after RNase digestion. In contrast, when this probe is annealed with synthetic R1A RNA, two fragments of 152 and 51 nucleotides are protected from RNase digestion (the 51-nucleotide fragment is not shown in Fig. 4). RNase protection with RNA from all brain regions generates an intact 266-nucleotide fragment as well as the smaller 152- and 51-nucleotide fragments (Fig. 4). These data indicate that all brain regions examined express NMDA-R1A and -R1B RNA. Similar results are obtained with RNA from pons/medulla, hypothalamus, striatum, and midbrain (data not shown). In most brain regions, the relative abundance of R1A to R1B RNA is ≈5:1. In contrast, this ratio is reversed in the cerebellum, where we observe five times more R1B than R1A RNA. Moreover, *in situ* hybridization with a 63-nucleotide exon probe reveals expression of NMDA-R1B in the granule and Purkinje cell layers of the cerebellum (data not shown). These data indicate that alternative splicing of NMDA-R1 RNA is regulated such that R1B RNA is far more abundant in the cerebellum than in other brain regions. Alternative RNA processing may therefore provide an explanation for the observation that NMDA receptors in cerebellar neurons exhibit properties different from those of other central neurons (34–36).

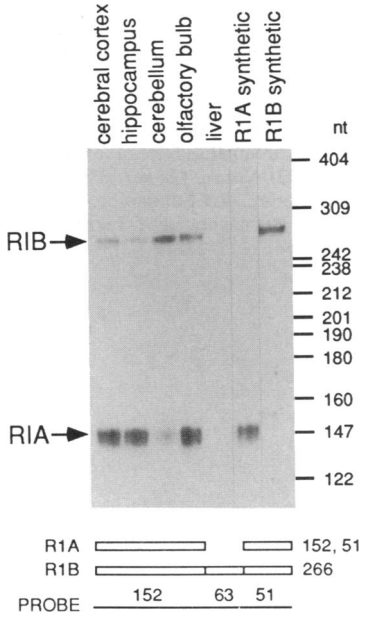


FIG. 4. R1A and R1B RNA in brain regions as measured by *in vitro* RNase protection. The $^{32}P$-labeled probe was hybridized to 10 $\mu$g of total RNA from rat (Sprague–Dawley, 4–6 weeks old) cerebral cortex, hippocampus, cerebellum, or olfactory bulb. Poly(A)$^+$ liver RNA (1 $\mu$g) and synthetic RNA (50 pg) from NMDA-R1A or -R1B were used as controls. Products of RNase protection were resolved on a denaturing 6% polyacrylamide gel. nt, Nucleotides. A schematic representation of expected RNase protection products is presented below the autoradiograph.

## DISCUSSION

These data demonstrate the presence of at least two structurally and functionally distinct NMDA receptor subunits that derive from the same gene by alternative splicing. Expression of either of the NMDA receptor subunits alone in oocytes results in an NMDA-evoked inward current with pharmacological and electrophysiological properties closely resembling those of the NMDA receptors observed in native neurons and in oocytes injected with brain RNA. Activation of the cloned receptors requires NMDA and glycine and both channels are blocked by $Mg^{2+}$ ions in a voltage-dependent manner. Thus, the complex properties exhibited by the NMDA receptor in neurons can be generated by the expression of a single receptor subunit. We have identified a third splicing variant, NMDA-R1C, in which a presumed exon from residues 846 to 882 in R1A is deleted (Fig. 1*A*) (15). Alternative splicing is also used by non-NMDA glutamate receptors to produce functionally distinct receptor subunits (37). RNA processing, therefore, serves as a general mechanism to generate functional diversity within the family of glutamate receptor subunits. At present, however, the physiologic consequences of these alternative splice choices remain unclear. The two alternatively spliced NMDA receptors display small, but significant, differences in their pharmacologic properties. NMDA-R1B is less sensitive than -R1A to both NMDA and glutamate. It is difficult to interpret the significance of these differences in agonist sensitivities since the concentration of glutamate in the cleft of the activated synapse is >200 $\mu$M (38), a value that far exceeds the $EC_{50}$ of both NMDA receptors. These differences in agonist sensitivity between R1A and R1B could, however, result in different spatial or temporal patterns of receptor activation at different synapses.

Recently, cDNAs were isolated encoding three additional receptor subunits, NMDA-R2A, -R2B, and -R2C, which derive from three independent genes (39, 40). When these cDNAs were expressed in *Xenopus* oocytes, no current could be elicited upon exposure to NMDA and glycine. However, when each of the NMDA-R2 subunits was mixed with NMDA-R1, the current amplitudes were on average 100-fold larger than the currents observed with NMDA-R1 alone (39, 40). These data suggest that the native NMDA receptor is likely to be a heteromultimer consisting of NMDA-R1 and at least one NMDA-R2 subunit. Moreover, whereas NMDA-R1 is ubiquitously expressed in the rat brain, the individual R2 subunits show overlapping but nonidentical distributions in different brain regions. Thus, different neurons may express distinct heteromultimers. Our data suggest that an additional level of diversity may result from alternative splicing. The expression of distinct NMDA receptors with different electrophysiological properties may be responsible for the dif-

ferent forms of activity-dependent synaptic plasticity in the mammalian brain. The initial cloning of an NMDA receptor subunit (14) and the subsequent isolation of additional NMDA receptor subunits (15, 39, 40) now permit a molecular analysis of NMDA receptor function and a genetic analysis of the role of the NMDA receptor in synaptic plasticity and neuronal degeneration *in vivo*.

We gratefully acknowledge Adriana Nemes for her professional technical assistance throughout the project. We thank Thomas M. Jessell and Amy MacDermott for their critical reading of this manuscript and Phyllis Kisloff for her help in its preparation. This work was supported by the Howard Hughes Medical Institute (R.A. and N.N.), Grant PO1 CA23767 (R.A.) from the National Institutes of Health (National Cancer Institute), and a National Institutes of Health Medical Scientist Training Program grant (N.A.S.).

1. Monaghan, D. T., Bridges, R. J. & Cotman, C. W. (1989) *Annu. Rev. Pharmacol. Toxicol.* **29**, 365–402.
2. Watkins, J. C., Krogsgaard-Larsen, P. & Honoré, T. (1990) *Trends Pharmacol. Sci.* **11**, 25–33.
3. Mayer, M. L. & Westbrook, G. L. (1987) *Prog. Neurobiol.* **28**, 197–276.
4. Johnson, J. W. & Ascher, P. (1987) *Nature (London)* **325**, 529–531.
5. Kleckner, N. W. & Dingledine, R. (1988) *Science* **241**, 835–837.
6. Nowak, L., Bregestovski, P., Ascher, P., Herbert, A. & Prschiantz, A. (1984) *Nature (London)* **307**, 462–465.
7. Jahr, C. E. & Stevens, C. F. (1987) *Nature (London)* **325**, 522–525.
8. Cul-Candy, S. G. & Usowicz, M. M. (1987) *Nature (London)* **325**, 525–528.
9. MacDermott, A. B., Mayer, M. L., Westbrook, G. L., Smith, S. J. & Barker, J. L. (1986) *Nature (London)* **321**, 519–522.
10. Mayer, M. L., Westbrook, G. L. & Guthrie, P. B. (1984) *Nature (London)* **309**, 261–263.
11. Gustafsson, B., Wigstrom, H., Abraham, W. C. & Huang, Y.-Y. (1987) *J. Neurosci.* **7**, 774–780.
12. Collingridge, G. L. & Singer, W. (1990) *Trends Pharmacol. Sci.* **11**, 42–48.
13. Choi, D. W. (1988) *Neuron* **1**, 623–634.
14. Moriyoshi, K., Masu, M., Ishii, T., Shigemoto, R., Mizuno, N. & Nakanishi, S. (1991) *Nature (London)* **354**, 31–37.
15. Yamazaki, M., Mori, H., Araki, K., Mori, K. & Mishina, M. (1992) *FEBS Lett.* **300**, 39–45.
16. Nakanishi, N., Shneider, N. A. & Axel, R. (1990) *Neuron* **5**, 569–581.
17. Hollman, M., O'Shea-Greenfield, A., Rogers, S. W. & Heinemann, S. (1989) *Nature (London)* **342**, 643–648.
18. Keinänen, K., Wisden, W., Sommer, B., Werner, P., Herb, A., Verdoorn, T. A., Sakmann, B. & Seeburg, P. H. (1990) *Science* **249**, 556–560.
19. Boulter, J., Hollman, M., O'Shea-Greenfield, A., Hartley, M., Deneris, E., Maron, C. & Heinemann, S. (1990) *Science* **249**, 1033–1037.
20. Bettler, B., Boulter, J., Hermans-Borgmeyer, I., O'Shea-Greenfield, A., Deneris, E. S., Moll, C., Borgmeyer, U., Hollmann, M. & Heinemann, S. (1990) *Neuron* **5**, 583–595.
21. Sakimura, K., Bujo, H., Kushiya, E., Araki, K., Yamazaki, M., Yamazaki, M., Meguro, H., Warashina, A., Numa, S. & Mishina, M. (1990) *FEBS Lett.* **272**, 73–80.
22. Werner, P., Voigt, M., Keinanen, K., Wisden, W. & Seeburg, P. H. (1991) *Nature (London)* **351**, 742–744.
23. Egebjerg, J., Bettler, B., Hermans-Borgmeyer, I. & Heinemann, S. (1991) *Nature (London)* **351**, 745–748.
24. Bettler, B., Egebjerg, J., Sharma, G., Pecht, G., Hermans-Borgmeyer, I., Moll, C., Stevens, C. F. & Heinemann, S. (1992) *Neuron* **8**, 257–265.
25. Sakimura, K., Morita, T., Kushiya, E. & Mishina, M. (1992) *Neuron* **8**, 267–274.
26. Julius, D., MacDermott, A. B., Axel, R. & Jessell, T. M. (1988) *Science* **241**, 558–564.
27. Imoto, K., Busch, C., Sakmann, B., Mishina, M., Konno, T., Nakai, J., Bujo, H., Mori, Y., Fukuda, K. & Numa, S. (1988) *Nature (London)* **335**, 645–648.
28. Hume, R. I., Dingledine, R. & Heinemann, S. F. (1991) *Science* **253**, 1028–1031.
29. Burnashev, N., Monyer, H., Seeburg, P. H. & Sakmann, B. (1992) *Neuron* **8**, 189–198.
30. Verdoorn, T. A. & Dingledine, R. (1988) *Mol. Pharmacol.* **34**, 298–307.
31. Kushner, L., Lerma, J., Zukin, R. S. & Bennett, M. V. (1988) *Proc. Natl. Acad. Sci. USA* **85**, 3250–3254.
32. Leonard, J. P. & Kelso, S. R. (1990) *Neuron* **4**, 53–60.
33. Patneau, D. K. & Mayer, M. L. (1990) *J. Neurosci.* **10**, 2385–2399.
34. Howe, J. R., Cull-Candy, S. G. & Colquhoun, D. (1991) *J. Physiol. (London)* **432**, 143–202.
35. Monaghan, D. T., Olverman, H. J., Nguyen, L., Watkins, J. C. & Cotman, C. W. (1988) *Proc. Natl. Acad. Sci. USA* **85**, 9836–9840.
36. Maragos, W. F., Penney, J. B. & Young, A. B. (1988) *J. Neurosci.* **8**, 493–501.
37. Sommer, B., Keinänen, K., Verdoorn, T. A., Wisden, W., Burnashev, N., Herb, A., Kohler, M., Takagi, T., Sakmann, B. & Seeburg, P. H. (1990) *Science* **249**, 1580–1585.
38. Clements, J. D., Lester, R. A. J., Jahr, C. E. & Westbrook, G. L. (1991) *Soc. Neurosci. Abstr.* **17**, 256.
39. Meguro, H., Mori, H., Araki, K., Kushiya, E., Kutsuwada, T., Yamazaki, M., Kumanishi, T., Arakawa, M., Sakimura, K. & Mishina, M. (1992) *Nature (London)* **357**, 70–74.
40. Moyer, H., Sprengel, R., Schoepfer, R., Herb, A., Higuchi, M., Lomeli, H., Burnashev, N., Sakmann, B. & Seeburg, P. (1992) *Science* **256**, 1217–1221.